6th IAHR International Meeting of the Workgroup on Cavitation and Dynamic Problems in Hydraulic Machinery and Systems, September 9-11, 2015, Ljubljana, Slovenia

RANS COMPUTATIONS OF A CAVITATING VORTEX ROPE AT FULL LOAD

Jean Decaix*

University of Applied Sciences and Arts, Western Switzerland, Switzerland.

Andres Müller

Laboratory for Hydraulic Machines, Ecole Polytechnique Fédérale de Lausanne, Switzerland.

François Avellan

Laboratory for Hydraulic Machines, Ecole Polytechnique Fédérale de Lausanne, Switzerland.

Cécile Münch

University of Applied Sciences and Arts, Western Switzerland, Switzerland.

ABSTRACT

Due to the massive penetration of alternative renewable energies, hydraulic power plants are key energy conversion technologies to stabilize the electrical power network using hydraulic machines at off design operating conditions. At full load, the axisymmetric cavitation vortex rope, developing in Francis turbine acts as an internal source of energy leading to instability called self-excited surge. 1D hydro-acoustic models are developed to predict such a phenomenon and to define the range of safe operating points for a hydropower plant. Such models involve several parameters that have to be calibrated. One way to calibrate these models consists of performing 3D computations of the cavitating vortex rope.

In the present work, a reduced scale model of Francis turbine has been investigated numerically in the framework of the Hyperbole research project at full load conditions. The main objective is to check the ability of the solver to compute a cavitating vortex rope in agreement with the experiment before using the simulations to calibrate the 1D models.

Two operating points have been computed using the Ansys CFX software. The operating points differ by their Thoma number whereas the other parameters remain the same. The flow is modelled using a homogeneous RANS approach. The phase change is taken into account using a transport equation for the gas volume fraction with a source term based on the simplified Rayleigh-Plesset equation. Turbulence is modelled using the k-ω SST model.

The numerical simulations are compared with experimental data. The comparisons focus on the pressure and velocity field in the draft tube. The results shows that the computations are able to capture some features of the vortex rope such as the wall pressure and the circumferential velocity field in the cone of the draft tube.

KEYWORDS

Cavitation, Francis turbine, Full load, Vortex rope, RANS.

* *Corresponding author:* University of Applied Sciences and Arts, Western Switzerland, Hydraulics Research Group, phone: +41276068835, email: jean.decaix@hevs.ch

1. INTRODUCTION

Due to the strong development of new green energies during the last ten years, the electrical network undergoes large fluctuations of the load since these energies are strongly dependent on the meteorological conditions. In order to manage the fluctuations of the load, other sources of energy are used to stabilize the grid. Among them, hydraulic power plants, which are also green energy, can be used due to their ability to respond quickly to a variation of the load. However, in order to inject the suitable power on the grid, the hydraulic turbines do not run at their best efficient point. In the case of Francis turbines, running the turbine at off design points provokes the development of flow instabilities such as the vortex rope in the draft tube. For instance, at full load, an axisymmetric vortex rope develops in the draft tube that promotes cavitation and large pressure surge. The pressure fluctuations can match the eigen frequencies of the mechanical parts of the turbine and provoke strong damages [1]. In order to increase the operating range of the Francis turbine, a better knowledge of the vortex rope is required. RANS computations can be used to investigate in details the flow behaviour in the draft tube. Furthermore, the computational results allow calibrating the 1D models used to simulate the behaviour of an entire hydraulic power plant [2].
The present study deals with computations of a vortex rope in a Francis turbine at full load. For a constant head and discharge, two Thoma numbers are investigated corresponding respectively to a stable and an unstable operating point. The results are compared with experimental data.

2. TEST CASE

A Francis turbine at model scale is considered for the computations. The operating points are defined by the following dimensionless coefficient:

- The specific speed ν:

$$\nu = \frac{\omega}{2^{3/4}\pi^{1/2}}\frac{Q^{1/2}}{E^{3/4}} \tag{1}$$

- The discharge factor Q_{ED}:

$$Q_{ED} = \frac{Q}{D^2 E^{1/2}} \tag{2}$$

- The speed factor n_{ED}:

$$n_{ED} = \frac{nD}{E^{1/2}} \tag{3}$$

- The Thoma number σ:

$$\sigma = \frac{NPSE}{E} \tag{4}$$

With Q the discharge ($m^3\ s^{-1}$), n the runner rotating frequency (Hz), ω the runner rotating speed (rad s^{-1}), E the specific hydraulic energy (J kg^{-1}), D the runner diameter (m) and $NPSE$ the Net Positive Suction Energy (J kg^{-1}). The values of the coefficients are gathered in Tab.1.

Operating points	ν (-)	Q_{ED} (-)	n_{ED} (-)	σ (-)
OP1	0.310	0.260	0.288	0.380
OP2				0.110

Table 1: Characteristics of the operating points.

The operating point OP1 is characterized by a stable vortex rope without cavitation. On the contrary, the operating point OP2 shows an unstable cavitating vortex rope. Moreover, a periodic shedding of cavitation bubbles from the trailing edge of the blades is observed.

3. MODELLING

The homogeneous RANS equations [3] with thermodynamic and mechanical equilibrium assumptions are used to solve the flow in the machine. Therefore, the phases are assumed to share the same pressure, velocity and temperature values. By neglecting the energy conservation equation, the equations to be solved are the mass conservation equation (Eq.5) and the momentum equation (Eq.6):

$$\frac{\partial \rho}{\partial t} + \nabla \cdot (\rho \vec{C}) = 0 \tag{5}$$

$$\frac{\partial \rho \vec{C}}{\partial t} + \nabla \cdot (\rho \vec{C} \otimes \vec{C}) = -\nabla p + \nabla \cdot (\bar{\bar{\tau}} + \bar{\bar{\tau}}_t) \tag{6}$$

With ρ the mixture density, $\vec{C}$ the mixture velocity, p the mixture pressure, $\bar{\bar{\tau}}$ and $\bar{\bar{\tau}}_t$ are respectively the viscous stresses and the turbulent stresses. The viscous stresses are computed assuming that the mixture is a Newtonian fluid (Eq.7).

$$\tau = \mu \left(\nabla \vec{C} + \nabla^t \vec{C} \right) \tag{7}$$

The turbulent stresses are computed using the Boussinesq's assumption (Eq.8) that introduces a turbulent viscosity μ_t.

$$\tau = \mu_t \left(\nabla \vec{C} + \nabla^t \vec{C} \right) - \frac{2}{3} \rho k \, \mathrm{tr}\left(\bar{\bar{I}} \right) \tag{8}$$

The turbulent viscosity is assessed using the *k-ω* SST model [4] that requires solving two additional conservation equations for the turbulent kinetic energy *k* and for the specific dissipation rate *ω*.

Cavitation is taken into account by solving a transport equation for the gas volume fraction r_g (Eq.9) [5]:

$$\frac{\partial r_g}{\partial t} + (\vec{C} \cdot \nabla) r_g = \frac{1}{\rho_g} (S_v + S_c) \tag{9}$$

With S_v and S_c the terms respectively responsible for the vaporisation and the condensation processes. They are derived (Eq.10 and Eq.11) from the simplified Rayleigh-Plesset equation that describes the dynamic behaviour of a spherical bubble.

$$S_v = F_v \frac{3 r_{nuc} (1 - r_g) \rho_g}{R_{nuc}} \sqrt{\frac{2}{3} \frac{|p_v - p|}{\rho_f}} \, \mathrm{sgn}(p_v - p) \quad \text{if } p < p_v \tag{10}$$

$$S_c = F_c \frac{3 r_g \rho_g}{R_{nuc}} \sqrt{\frac{2}{3} \frac{|p_v - p|}{\rho_f}} \, \mathrm{sgn}(p_v - p) \quad \text{if } p > p_v \tag{11}$$

F_v, F_c, r_{nuc} and R_{nuc} are unknown parameters that have to be calibrated. The default values are used in the present study [6].

$$F_v = 50 \qquad F_c = 0.01 \qquad r_{nuc} = 5e^{-4} \qquad R_{nuc} = 10^{-6} \mathrm{m} \tag{12}$$

The saturated vapour pressure p_v is set to 1'800 Pa.

4. NUMERICAL SET UP

The complete domain including the spiral case, the stay vanes, the guide vanes, the runner and the draft tube is considered for the simulations (Fig.1). A structured mesh (Fig.2) is built for

each part of the computational domain. The total number of nodes is slightly above 10 million (Tab.2).
The flow rate is imposed at the inlet, whereas the pressure is set at the outlet. For each case, the outlet pressure is adjusted to match the experimental Thoma number. A no slip condition is set at the solid walls. To compute the turbulent stresses in the first cell layer close to a wall, a wall law is used.
Steady computations are carried out with a stage condition set at the interfaces between the stationary and the rotating domains. The stage interface consists of performing a circumferential averaging of the fluxes through bands on the interface.

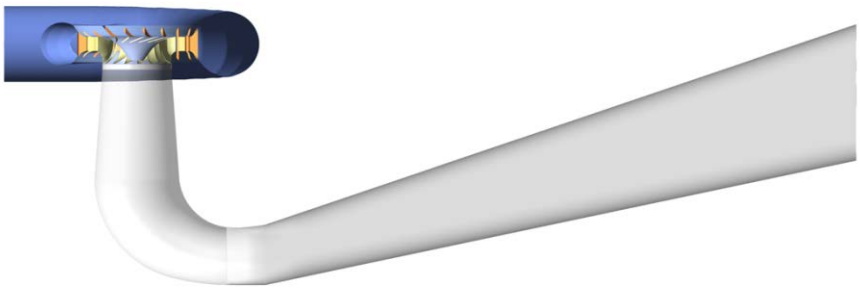

Fig 1: Computational domain.

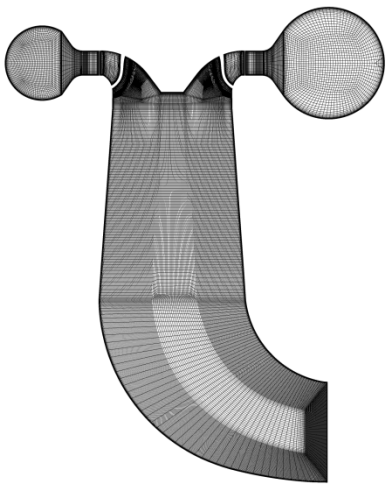

Fig 2: Mesh in a meridional plane.

Part	Number of nodes (in million)
Spiral Case	1.69
Stay Vanes and Guides Vanes	3.17
Runner	2.63
Draft Tube	3.10
Total	**10.59**

Table 2: Number of nodes for each part of the mesh.

5. RESULTS

The global performances of the turbine are given respectively in Tab.3 and Tab.4 for the two operating points. The computations overestimate the efficiency η, the speed factors n_{ED} and

the discharge factors Q_{ED} compared to the experimental results. The differences for the speed and discharge factors are mainly due to an underestimation of the specific energy. This difference can be partially explained by the achievement of steady computations with a stage averaging. For the efficiency, not all the losses are considered in the simulations.

Parameters	Experiment	CFD
η (-)	0.876	0.907
n_{ED} (-)	0.288	0.297
Q_{ED} (-)	0.259	0.269

Table 3: Global performances of the turbines at OP1.

Parameters	Experiment	CFD
η (-)	0.871	0.896
n_{ED} (-)	0.288	0.301
Q_{ED} (-)	0.264	0.272

Table 4: Global performances of the turbines at OP2.

For the tests, the wall pressure is measured in two cross sections located along the straight part of the draft tube (Fig.3). To compare the experimental data with the computational results, a cavitation number σ_u is defined by:

$$\sigma_u = \frac{\overline{p} - p_v}{0.5\rho U_1^2} \tag{13}$$

With $\bar{p}$ the wall mean pressure in the section considered and U_1^2 the rotating velocity at the outer diameter at the runner outlet. Tab.5 and Tab.6 gather the experimental and the numerical values for respectively the operating points OP1 and OP2. Except for OP2 at the upper section, the differences between the computational and the experimental data are lower than 2%.

	Experiment	Computation
σ_u (upper section)	0.858	0.867
σ_u (lower section)	0.903	0.916

Table 5: Value of the cavitation number σ_u in the draft tube for OP1.

	Experiment	Computation
σ_u (upper section)	0.184	0.192
σ_u (lower section)	0.240	0.239

Table 6: Value of the cavitation number σ_u in the draft tube for OP2.

Since no cavitation is observed at OP1, the vortex rope is visualized using a pressure iso-surface (Fig.3). On the contrary, at OP2, the cavitating vortex rope is visualized using an iso-surface of the gas volume fraction (Fig.4, left). Cavitation on the blade suction sides is captured numerically, which can be related to the periodic shedding of cavitating bubbles observed experimentally in the draft tube. Compared to the experiment (Fig.4, right), the cavity volume is underestimated by the computation. Once again the achievement of a steady computation as well as the mesh resolution can explain the low volume.

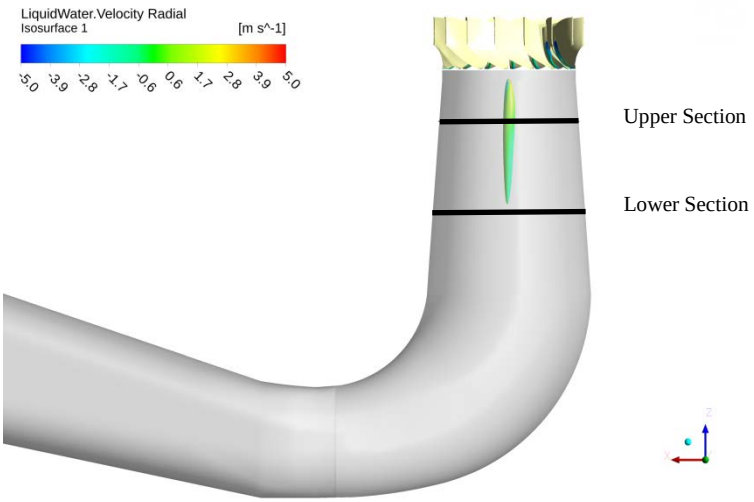

Fig 3: Pressure iso-surface (p = 60‘000 Pa). OP1.

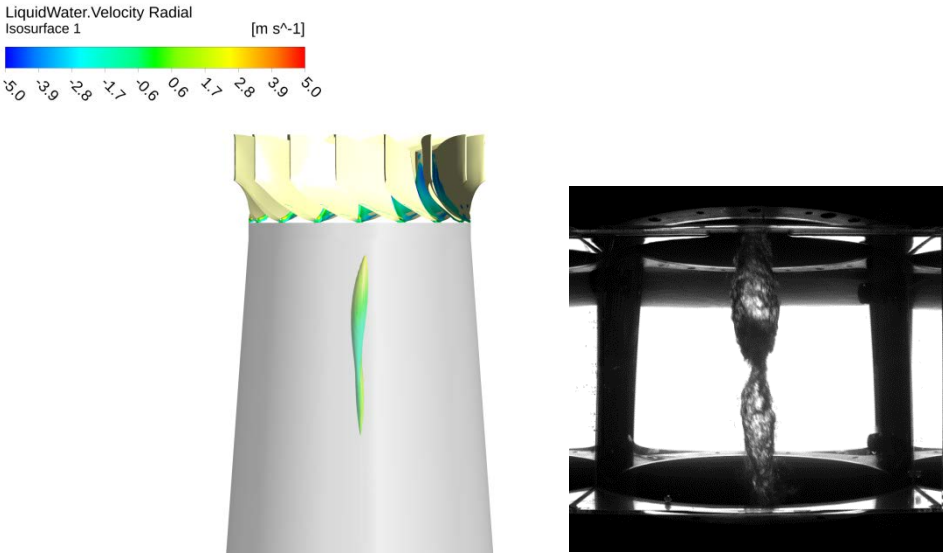

Fig 4. Left: Iso-surface of the gas volume fraction (r_g = 0.1).
Right: experimental picture of the vortex rope. OP2.

The tangential velocity component C_u in the upper and lower sections has been surveyed by LDV for the operating point OP2. It is compared in Fig.5 and Fig.6 with the numerical data using a dimensionless representation with: $r^* = \frac{r}{D}$ and $C_u^* = \frac{C_u}{Q/(\frac{\pi D^2}{4})}$. Close to the wall ($r^* < -0.35$), the computation profile is in agreement with the experimental results. In the vortex core, the sharp decrease is also well captured. On the contrary, in the region between $r^* > -0.35$ and $r^* < -0.1$, the computation underestimates the tangential velocity. However, at the lower section, the computation is able to capture the shape of the velocity profile with a slight decrease follows by a peak of the circumferential velocity at the boundary between the liquid and vapour regions.

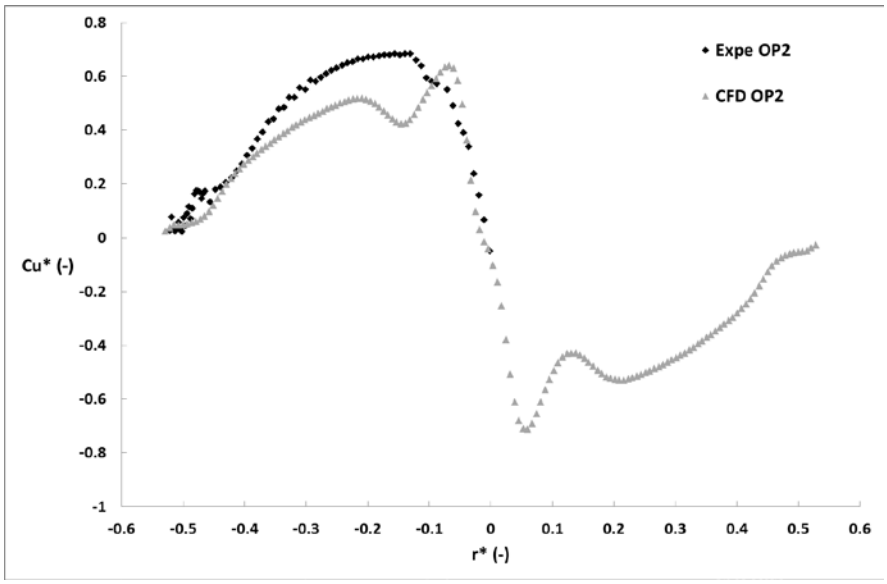

Fig 5: Dimensionless circumferential velocity Cu in the upper section.*

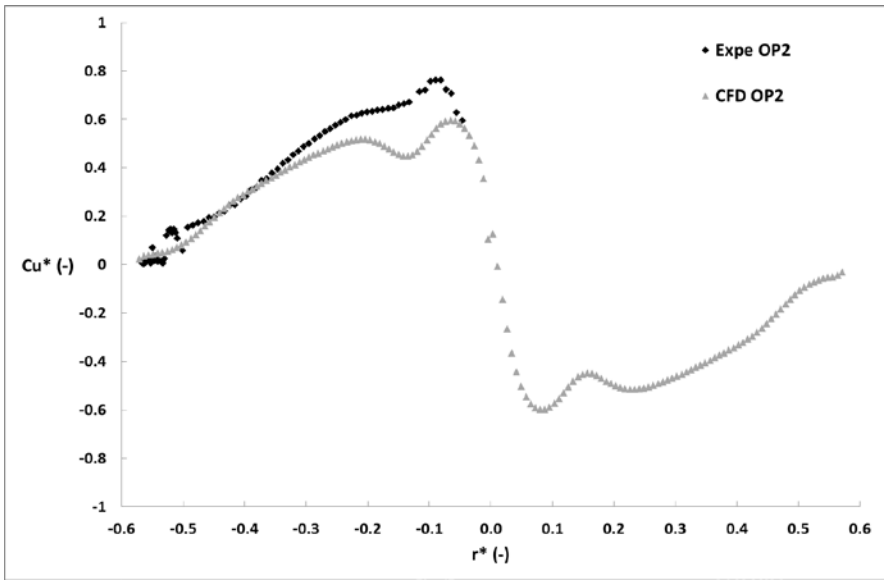

Fig 6: Dimensionless circumferential velocity Cu in the lower section.*

6. CONCLUSION

An investigation of a vortex rope at full load has been carried out by using homogeneous RANS numerical simulations. Two steady simulations are performed for both at stable operating and unstable operating conditions. The global performance of the turbine shows an underestimation of the specific energy provided by the computations compared to the experimental results data. However, the wall pressure the draft tube is well captured. Moreover, at the unstable operating point, a qualitative agreement regarding the circumferential velocity field is observed. However, the circumferential velocity field is underestimated at the boundary between the liquid and the vapours zones.

The differences between the experimental data and the computations can be explained by the achievement of steady computations and the use of a too coarse mesh inside the vortex rope. These two points will be investigated in a future work. In addition outlet forced pressure fluctuations will be imposed to provide the relevant data used to calibrate the 1D models.

7. ACKNOWLEDGEMENTS

The research leading to the results published in this paper is part of the HYPERBOLE research project, granted by the European Commission (ERC/FP7-ENERGY-2013-1-Grant 608532).

8. REFERENCES

[1] Koutnik, J., Nicolet, C., Schohl, G. and Avellan, F. "Overload Surge Event in a Pumped-Storage Power Plant," *23rd IAHR Symp. Hydraul. Mach. Syst. Oct. 17-21*, vol. 1, no. October, pp. 1–15, 2006.

[2] Alligné, S., Nicolet, C., Tsujimoto, Y., and Avellan,F., "Cavitation Surge Modelling in Francis Turbine Draft Tube," *J. Hydraul. Res.*, vol. 52, no. 3, pp. 1–13, 2014.

[3] Brennen, C.E. *Cavitation and bubble dynamics*. Oxford University Press, New York, 1995.

[4] Menter, F.R. "Two-equation Eddy-viscosity turbulence models for engineering applications," *AIAA Journal*, 32 (8), 1994, pp. 269-289.

[5] Zwart, P., Gerber, A., and Belamri, T. "A two-phase flow model for predicting cavitation dynamics," *Fifth Int. Conf. Multiph. Flow, Yokohama, Japan, May 30 - June 3*, no. 152, 2004.

[6] Bakir, F., Rey, R., Gerber, A.G., Belamri, T., and Hutchinson, B. "Numerical and Experimental Investigations of the Cavitating Behavior of an Inducer," *Int. J. Rotating Mach.*, vol. 10, no. 1, pp. 15–25, Jan. 2004.

9. NOMENCLATURE

C_u	(m s^{-1})	circumferential velocity
D	(m)	runner diameter
E	(J kg^{-1})	specific hydraulic energy
n	(Hz)	runner rotating frequency
n_{ED}	(-)	speed factor
$NPSE$	(J kg^{-1})	Net Positive Suction Energy
p	(Pa)	pressure
p_v	(Pa)	saturated vapour pressure
Q	(m^3 s^{-1})	discharge
Q_{ED}	(-)	discharge factor
r	(m)	radius
r_g	(-)	gas volume fraction
r_{nuc}	(-)	volume fraction of the nucleation sites
R_{nuc}	(m)	nucleation site radius
U_1	(m s^{-1})	rotating velocity at the outer diameter at the runner outlet
μ	(kg m^{-1} s^{-1})	molecular dynamic viscosity
μ_t	(kg m^{-1} s^{-1})	turbulent dynamic viscosity
ν	(-)	specific speed
ρ_g	(kg m^{-3})	gas density
ρ_f	(kg m^{-3})	liquid density
σ	(-)	Thoma number
σ_u	(-)	Cavitation number based on the runner peripheral velocity
ω	(rad s^{-1})	runner rotating speed